Computational and Structural Biotechnology Journal 19 (2021) 2664–2675

COMPUTATIONAL AND STRUCTURAL BIOTECHNOLOGY JOURNAL

journal homepage: www.elsevier.com/locate/csbj

A novel bioengineered fragment peptide of Vasostatin-1 exerts smooth muscle pharmacological activities and anti-angiogenic effects via blocking VEGFR signalling pathway

Ran Wei [a,b], Qiushuang Wu [b,c], Nana Ai [d], Lei Wang [e], Mei Zhou [e], Chris Shaw [e], Tianbao Chen [e], Richard Dequan Ye [f], Wei Ge [d], Shirley W.I. Siu [g], Hang Fai Kwok [b,c,*]

[a] CCZU-JITRI Joint Bio-X Lab, School of Pharmacy & School of Medicine, Changzhou University, Changzhou, China; Cancer Centre, Faculty of Health Sciences, University of Macau, Avenida de Universidade, Taipa, Macau SAR
[b] Institute of Translational Medicine, Faculty of Health Sciences, University of Macau, Avenida de Universidade, Taipa, Macau SAR, China
[c] Cancer Centre, Faculty of Health Sciences, University of Macau, Avenida de Universidade, Taipa, Macau SAR; MoE Frontiers Science Center for Precision Oncology, University of Macau, Avenida de Universidade, Taipa, Macau SAR, China
[d] Centre of Reproduction, Development and Aging (CRDA), Faculty of Health Sciences, Avenida de Universidade, University of Macau, Macau SAR, China
[e] Natural Drug Discovery Group, School of Pharmacy, Queen's University Belfast, Northern Ireland, United Kingdom
[f] School of Life and Health Sciences, The Chinese University of Hong Kong (Shenzhen), Shenzhen, China
[g] Department of Computer and Information Science, Faculty of Science and Technology University of Macau, Avenida de Universidade, Taipa, Macau SAR, China

ARTICLE INFO

Article history:
Received 8 March 2021
Received in revised form 30 April 2021
Accepted 1 May 2021
Available online 3 May 2021

Keywords:
Chromogranin A
Vasostatin-1
Anti-angiogenesis
VEGFR2

ABSTRACT

Chromogranin A (CgA) is a hydrophilic glycoprotein released by post-ganglionic sympathetic neurons. CgA consists of a single peptide chain containing numerous paired basic residues, which are typical cleavage sites in prohormones to generate bioactive peptides. It is recognized as a diagnostic and prognostic serum marker for neuroendocrine tumours. Vasostatin-1 is one of the most conserved regions of CgA and has diverse inhibitory biological activities. In this study, a novel peptide fragment that contains three typical functional structures of Vasostatin-1 was synthesized. This unique bioengineered Vasostatin-1 Derived Peptide (named V1DP) includes a highly conserved domain between vertebrate species in its N-terminal region, comprising a disulphide bridge formed by two cysteine residues at amino acid positions 17 and 38, respectively. Besides, V1DP contains two significant tripeptide recognition sequences: the amino acid triplets, RGD and KGD. Our data demonstrated that V1DP could induce a dose-dependent relaxation of rat arterial smooth muscle and also increase the contraction activity of rat uterus smooth muscle. More importantly, we found that V1DP inhibits cancer cell proliferation, modulate the HUVEC cell migration, and exhibit anti-angiogenesis effect both in *vitro* and in *vivo*. We further investigated the actual mechanism of V1DP, and our results confirmed that V1DP involves inhibiting the vascular endothelial growth factor receptor (VEGFR) signalling. We docked V1DP to the apo structures of VEGFR2 and examined the stability of the peptide in the protein pockets. Our simulation and free energy calculations results indicated that V1DP can bind to the catalytic domain and regulatory domain pockets, depending on whether the conformational state of the protein is JM-in or JM-out. Taken together, our data suggested that V1DP plays a role as the regulator of endothelial cell function and smooth muscle pharmacological homeostasis. V1DP is a water-soluble and biologically stable peptide and could further develop as an anti-angiogenic drug for cancer treatment.

1. Introduction

Chromogranin A (CgA) is a hydrophilic glycoprotein released by post-ganglionic sympathetic neurones and was first discovered in catecholamine-containing adrenal chromaffin cells [1]. It is co-stored and co-released in the secretory granules of endocrine, neuroendocrine, and immune cells [2–4]. CgA consists of a single

* Corresponding author at: Cancer Centre, Faculty of Health Sciences, University of Macau, Avenida de Universidade, Taipa, Macau SAR, China.
E-mail address: hfkwok@um.edu.mo (H.F. Kwok).

https://doi.org/10.1016/j.csbj.2021.05.003

peptide chain containing numerous paired basic residues, which are typical cleavage sites in prohormones to generate bioactive peptides [5]. CgA-related polypeptides are detected in the blood of patients with neuroendocrine tumors, renal failure, heart failure, rheumatoid arthritis, hypertension and inflammatory bowel disease [6]. In human Full-length CgA and CgA-derived peptides are variously expressed with pathological conditions and exert distinctive paracrine, autocrine and endocrine functions [7]. For example, in human CgA derived peptide, Vasostatin-1 (CgA1–76), Pancreastatin ($CgA_{250\text{-}301}$), Catestatin ($CgA_{352\text{-}372}$) are the well-recognized CgA authentic products [3,5,6]. Catestatin is diminished in genetic hypertension, whereas the full length of CgA is overexpressed [6]. And in rodents, Catestatin could sensitize the insulin function and decrease hypertension, obesity, cardiac contractility, atherosclerosis and inflammation, while the Pancreastatin exerts an opposite function of Catestatin [6,8,9]. Interestingly, the N-terminal fragment Vasostatin-1 is a water-soluble and biologically stable peptide and has revealed the potential of antiangiogenetic and modulate fibroblast and endothelial cell adhesion. While CgA fragments lacking the C-terminal region showed proangiogenic activity and induce tumor growth [6,7,9]. The capability of CgA in regulating cell adhesion may be crucial in the metastasis of neuroendocrine tumours as its abnormal circulating level in many neuroendocrine tumour tissues [10]. Overall, the CgA system, consisting of full-length CgA and its fragments, is emerging as an important and complex player in cardiovascular, immunometabolic, and cancer regulation.

The determination of these peptides/proteins primary structures, revealing their high degree of structural conservation across species, suggests that they may perform an important and fundamental biological role. Vasostatin-1 is one of the most conserved regions of CgA and has diverse inhibitory biological activities. In the amino acid sequence of Vasostatin-1, the presence of two significant tripeptide recognition sequences has been demonstrated: the amino acid triplets, Arg-Gly-Asp (RGD), residues (43–45) and Lys-Gly-Asp (KGD), residues (9–11). These motifs are known to play a major inhibitory role in cell adhesion and possibly angiogenesis. Some research related to the RGD motif peptides has demonstrated some typical inhibitory characteristics on platelet aggregation, angiogenesis and tumour growth [1,11]. The tripeptide RGD is also found in the sequences of a number of other proteins, where it has been shown to play a role in cell adhesion [12].

In this study, a novel peptide fragment that contains three typical functional structures of Vasostatin-1 was synthesized. This fragment is a selected fragment of Vasostatin-1, and also sequences as the N-terminal 8–47 fragment of CgA. This unique bioengineered Vasostatin-1 Derived Peptide (named V1DP) includes the three typical functional structures within Vasostatin-1. It has been shown that V1DP contains a highly conserved domain between vertebrate species in its N-terminal region, comprising a disulphide bridge formed by two cysteine residues at amino acid positions 17 and 38. In addition, the sequence of V1DP contains two significant tripeptide recognition sequences: the amino acid triplets, RGD and KGD. This novel Vasostatin-1 derived has been characterized through various functional screening such as the MTT cell viability assay, haemolysis assay and smooth muscle bioassay. It was observed that V1DP induced a dose-dependent relaxation of rat arterial smooth muscle and also induced an increase in the contraction activity of rat uterus smooth muscle preparations. We also found its potential role in inhibiting cancer cell proliferation, modulating the HUVEC cell migration, exhibiting anti-angiogenesis effect both in *vitro* and in *vivo*. We further investigated the potential mechanism of the anti-angiogenesis effect of V1DP through western blot. The results indicated the anti-angiogenesis effect of V1DP might involve the inhibition of VEGFR signaling. Such data would be important clues to explain the mechanism of the biological function of Vasostatin-1 through these structure/activity studies.

2. Method

2.1. Peptide synthesis and purification

Peptides were synthesized using solid-phase Fmoc chemistry by means of a PS4 automated solid-phase peptide synthesizer (Protein Technologies, Inc., AZ, USA). The purification of the synthetic peptides was analyzed by both reverse-phase HPLC and MALDI-TOF mass spectrometry. The HPLC column C18 (Phenomenex C-18, 25 cm × 0.45 cm) was washed by Buffer B (0.05%/29.95/70.00 (TFA/water/Acetonitrile) (v/v/v)) for approximately 30–60 min and then it was equilibrated in Buffer A (trifluoroacetic acid (TFA)/water (0.05/99.95, v/v) for 1 h. Synthetic peptides were dissolved in Buffer A at a concentration of 1 mg/ml then injected onto the HPLC system and peptides were eluted using a gradient formed from 0.05/99.95 (v/v) TFA/water to 0.05/19.95/80.0 (v/v/v) TFA/water/acetonitrile in 80 min at a flow rate of 1 mL/min. For MALDI-TOF mass spectrometry, matrix solution (α-cyano-4-hydroxycinnamic acid (CHCA)) was prepared as a 10 mg/ml solution of CHCA in acetonitrile/TFA/Water (50/0.05/49.95, v/v/v).

The primary structures of the major products (>90%) in each synthesis mixture, were finally confirmed by LCQ-Fleet^{TM} electrospray ion-trap mass spectrometer. In the ESI source, nitrogen sheath and auxiliary gas flows were maintained at 30 and 10 arbitrary units as set by the software, respectively. The resulting fragment ion profile was then searched using the SEQUEST algorithm in the Thermo Scientific Proteome Discoverer 1.0 software Sequest algorithm (ThermoFinnigan, San Jose, California, USA) against a customized FASTA database of related sequences.

2.2. Rat smooth muscle bioassay

Female Wistar rats (200–300 g) were applied and sacrificed followed the principle of institutional animal experimentation ethics and UK animal research guidelines. All of the procedures involved in this study was approved by IACUC of Queen's University Belfast. The tail artery and uterus were generated as described previously [13,14]. The peptide was diluted in Kreb's solution to a range of concentrations from 10^{-11} to 10^{-5} M for the construction of dose–response curves. These peptides were added to the smooth muscle preparations in increasing concentrations followed by 5 min washing and 5 min equilibration periods between each dose. Changes in tension of the smooth muscle preparations were recorded and amplified through force transducers connected to a PowerLab System (AD Instruments Pty Ltd.).

2.3. Haemolysis assays

Forty percent of (packed cell volume) fresh horse blood (TCS Biosciences Ltd. Buc kingham, UK) was used [15]. 4% of horse erythrocytes were prepared and incubated with a range of concentration of peptide for 120 min. The incubation of erythrocytes with 1% (v/v) Triton X-100 and with PBS were used as positive and negative control, respectively. The supernatants were measured by Optical density (OD) at 550 nm using a Synergy HT plate reader.

2.4. Cell culture

HCT116, DLD-1 and CCD-18CO were purchased from American Type Culture Collection (ATCC). DKS8 and HKE3 were gifts from Prof. Senji Shirasawa's Laboratory [16]. Human umbilical vein

endothelial cells (HUVEC) were purchased from Thermo Fisher Scientific. HCT116, DLD-1, HKE3, DKS8 and CCD-18CO were maintained in DMEM/F-12 (Gibco: Cat. no. 1320033) with 10% foetal bovine serum and 1% penicillin/streptomycin, HUVEC cell line was grown in Medium 200 supplemented with low serum growth supplement (LSGS) (Thermo Fisher Scientific, Waltham, MA). All cell lines were incubated at 37 °C, 5% CO_2.

2.5. MTT cell viability assays

The synthetic peptides were analyzed by the MTT-based in vitro toxicology test [14,15]. The cells were seeded to the required numbers (5×10^3 cells per well) in a 96-well plate before further testing. After 24 h incubation, the medium in each well was removed FBS-free medium then further incubated for 12 h. Cells were treated with different peptide concentrations range from 10^{-5} to 10^{-12} M with serum-free medium for 24 h. Afterwards, 10 μl (5 mM) MTT solution (Sigma, UK) were added to each well, and the plate was incubated for 4 h at 37 °C, 5% CO_2. The medium of each well gently removed, and 100 μl of DMSO was later added to each well and mixed thoroughly until all the formazan crystals were dissolved. The plates were then placed in an ELx808™ Absorbance Microplate Reader (BioTek, USA) and the absorbance measured at λ550 nm.

2.6. Wound healing cell migration assay

HUVEC were seeded in a 96-well Microplate (Image Lock plates, Essen Bioscience) at the density of 1×10^4 cells/well and then incubated overnight, then changed the medium with and without peptide added for 6 h before wounding by WoundMaker™ (Essen BioScience). The cell plate was placed into the IncuCyte ZOOM (Essen BioScience) for 24 h and scanned every 2 h. The relative wound density was calculated by IncuCyte ZOOM Software [16].

2.7. Endothelial cell tube formation assay

HUVEC cells were treated with and without peptide added medium for 6 h. Then the cell lines were seeded into a 15-well m-Slide angiogenesis chamber (ibidi, Planegg, Germany) coated with 10 μl Matrigel (BD Biosciences) and calculated with 1.5×10^3/well. After incubation for 18 h, morphological changes of HUVECs and tube formation were visualized and photographed using the EVOS Cell Imaging System.

2.8. Western blots assay

The detailed protocol referred to a previous publication [16]. The cell line samples were lysed with ice-cold RIPA lysis buffer contained with protease inhibitor (Complete EDTA-free, #10634200, Roche) and phosphatase inhibitor (PhosSTOP, #04906837001, Roche) and centrifuged at 20 000 × g for 30 min at 4 °C. Supernatants were collected and quantified using Pierce BCA Protein Assay Kit (#23225). All samples were dissolved in LDS sample buffer and reducing agent (Life Technologies) and heated for 5 min at 95 °C. An equal concentration of proteins was electrophorized and separated with TGX Stain-FreeTM FastCastTM Acrylamide Kit, 12% and transferred to a polyvinylidene difluoride (PVDF) membrane (Bio-Rad; Hercules, CA). Blocking was carried out with 5% non-fat milk, 0.1% Tween for 1 h in room temperature. Then the blots were incubated overnight with primary antibody at 4 °C. After washing with PBST for 10 mins three times, the membranes were incubated with secondary antibody for 1-hour prior. Finally, the bands were visualized by ChemiDoc MP Imaging System (Bio-Rad). with adding the chemiluminescent HRP substrate reagent (1:1) (Immobilon Western, WBKLS0500, Millipore). Primary antibodies used were phospho-ERK1/2 (Thr202/Tyr204) (1:1000, #9101, CST), total ERK1/2 (1:1000, #9102, CST), Phospho-VEGF Receptor 2 (Tyr1175) (1:1000, #2478S, CST), VEGF Receptor 2 (1:1000, #2479, CST), GAPDH (1;1000,#2118, CST).

2.9. Zebrafish angiogenesis assay

The *Tg*(*fli1a*:EGFP) transgenic zebrafish were used in this study, and all the procedures were approved by the Animal Research Ethics Committee of the University of Macau. The detailed protocol was described in our previous study [17]. The fish were maintained in the ZebTEC multilinking rack system (Tecniplast; Buguggiate, Italy) at 28 °C on 14 h light:10 h dark photoperiod. Zebrafish embryos at 2 hpf (hours after fertilization) were placed in a dish with 30 mL system water containing 0.1% 1-phenyl 2-thiourea (PTU) to suppress pigment cell development. At 24 hpf, the eggshells (chorion) were gently removed with forceps, and the embryos were transferred to a 24-well plate at a density of 15 embryos/1 mL system water per well. Peptides were prepared with different concentrations and injected into the embryos at 9.2 nl/embryo, and the intersegmental vessels (ISVs) and subintestinal vessels (SIVs) of the embryos were observed at 48 (24-h treatment) and 72 hpf respectively.

2.10. Molecular model construction

The three-dimensional structure of V1DP was predicted using the PEPFOLD3 server [18]. The best model was selected based on the sOPEP energy and was submitted to MD to obtain an equilibrated structure. For the protein receptor, we chose two different ligand-bound crystal structures of the human VEGFR2 kinase domain to investigate how the peptide binds. The two structures are different in the way that the juxtamembrane (JM) domain is oriented. For PDB 4AGD, the JM domain is inserted into the regulatory domain pocket (RDP) and packed close to the DFG domain (the JM-in state). On the contrary, for PDB 4ASD, the JM domain is rearranged out of the RDP (the JM-out state), thereby increasing the RDP cavity volume. We followed these steps to prepare the protein models for peptide docking: In each case, the co-crystallized ligand was first removed, and the missing N-terminal residues were modeled using the Swiss-Model homology modeling server [19]. As the kinase insert domain (57 residues) is missing in the crystal structure, we followed a previous study [20] to construct five alanine to join residues Tyr938 to Tyr996. Finally, the remodeled protein was subjected to 200 ns MD simulation and then clustering analysis to select receptor conformations for peptide docking.

2.11. Molecular docking of V1DP with VEGFR2

BIOVIA Discovery Studio 2017 R2 (Biovia, San Diego, CA, USA) was used to carry out the molecular docking simulation. ZDOCK of Discovery Studio with ZRANK (ranks docked poses) was used by the following parameters: Angular step size as 15; RMSD cutoff as 6.0; interface cutoff as 9.0; the maximum number of clusters as 60, then RDOCK procedure was used to refine the docked poses by using the Chemistry at Harvard Macromolecular Mechanics (CHARMM) force field [14,21]. In addition to Discovery Studio, other docking methods, HPEPDOCK, AutoDock Vina, and ZDOCK were tried, but the peptide was docked with either unfolded conformation or docked with too low-affinity binding poses.

2.12. Molecular dynamics simulation of protein-peptide complex

Selected protein-peptide complexes from the results of molecular docking were subjected to MD simulations. All MD simulations

were performed using GROMACS 2019 and the CHARMM36m force field. The complex was placed in the centre of the TIP3P water box with a padding distance of 1.2 nm to the box boundary and was neutralized with counter ions Na^+Cl^-. The system was energy minimized using the steepest descent algorithm and subsequently equilibrated under an NVT ensemble for 2 ns. The final trajectory was run under an NPT ensemble with a temperature of 300 K and pressure of 1 bar. We followed the simulation conditions as provided in the CHARMM-GUI [22] solution builder output. For analysis, atomic coordinates and energies were recorded every 10 ps. Binding free energy calculations were carried out using the program gmx_MMPBSA with the following parameters: igb = 5, saltcon = 0, entropy = 2, entropy_seg = 25, entropy_temp = 300. Forty frames were extracted from the last 40 ns of simulation for the calculation. The values of energy differences from the Complex-Receptor-Ligand section in the final output file were collected and analyzed.

2.13. Statistical analysis

Dose-response curve and bar graphs were plotted with Prism 7 (GraphPad Software, La Jolla, CA). All experiments were performed in triplicate. Data are expressed as means ± standard deviation (SD). Statistical differences of the data between control and treatment groups using one-way ANOVA, and the P values <0.05 were considered statistically significant.

3. Results

3.1. Interspecies comparison and structural characterization of V1DP.

V1DP (NKGDTEVMKCIVEVISDTLSKPSPMPVSQECFETLRGDER) has shown high interspecies conservation compared to humans rat, mouse, bovine and pig (Fig. 1A). The N-terminal tripeptide KGD sequence and the Cys17–Cys38 disulfide bridge is highly-conserved in human, rat, mouse bovine and pig. The C-terminal RGD sequence is replaced by QGD in the rat and mouse, which has raised some arguments against its functional role. The sequence of V1DP has been chemically synthesized with a modification of disulfide bridge at Cys17–Cys38, and mass spectra validated the purity with an observed MW4467.60 (Fig. 1B), and the sequence was validated through MS/MS (Fig. 1C).

3.2. Smooth muscle pharmacology assay and haemolysis assays

Specifically, V1DP induced a dose-dependent relaxation of rat arterial smooth muscle (EC_{50} 2.34 nM, Fig. 2A) and exhibited contraction of rat uterus smooth muscle preparations (EC_{50} 0.31 μM, Fig. 2B). The results of the haemolysis assays indicated all of the peptides tested had no observable haemolytic activity in the concentration range investigated (Fig. 2C).

3.3. Cell viability and proliferation assay

The cell proliferation assay was carried out with MTT cell viability assay. HCT116, HKE-3, DLD-1, DKS-8, CCD-18CO and HUVEC were treated with V1DP peptide with different concentration. The data were analyzed to establish comparative IC_{50} values, and dose–response curves were then constructed using the best-fit algorithm (non-linear regression). Specifically, the comparative IC_{50} values of V1DP on the human cancer cell lines and normal fibroblast cells were: HCT116 (IC_{50} 9.6 nM), HKE-3 (IC_{50} 26 nM), DLD-1 (IC_{50} 62 nM), DKS-8(IC_{50} 35 nM), CCD-18CO(2.596 μM), and HUVEC (0.154 μM). The data indicated that V1DP has different anti-proliferative efficacy and selective cytotoxicity against cancer cell growth and normal cells with the IC_{50} magnitude from nanomolar to micromolar (Fig. 3).

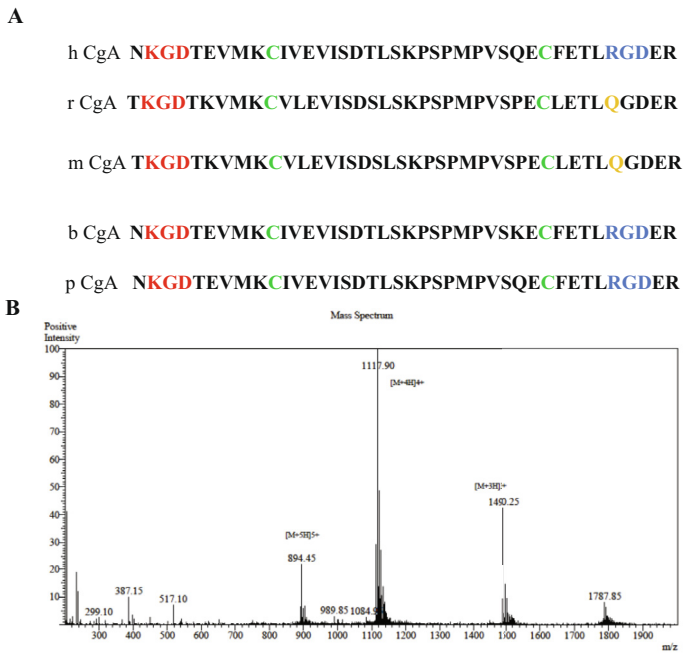

C

#1	b(1+)	b(2+)	b(3+)	Seq.	y(1+)	y(2+)	y(3+)	#2
1	115.05021	58.02874	39.02159	N				40
2	243.14518	122.07623	81.71991	K	4354.10759	2177.55743	1452.04071	39
3	300.16665	150.58696	100.72707	G	4226.01262	2113.50995	1409.34239	38
4	415.19360	208.10044	139.06938	D	4168.99115	2084.99921	1390.33523	37
5	516.24128	258.62428	172.75194	T	4053.96420	2027.48574	1351.99292	36
6	645.28388	323.14558	215.76614	E	3952.91652	1976.96190	1318.31036	35
7	744.35230	372.67979	248.78895	V	3823.87392	1912.44060	1275.29616	34
8	875.39280	438.20004	292.46912	M	3724.80550	1862.90639	1242.27335	33
9	1003.48777	502.24752	335.16744	K	3593.76500	1797.38614	1198.59318	32
10	1106.49696	553.75212	369.50384	C	3465.67003	1733.33865	1155.89486	31
11	1219.58103	610.29415	407.19853	I	3362.66084	1681.83406	1121.55846	30
12	1318.64945	659.82836	440.22133	V	3249.57677	1625.29202	1083.86377	29
13	1447.69205	724.34966	483.23553	E	3150.50835	1575.75781	1050.84097	28
14	1546.76047	773.88387	516.25834	V	3021.46575	1511.23651	1007.82677	27
15	1659.84454	830.42591	553.95303	I	2922.39733	1461.70230	974.80396	26
16	1746.87657	873.94192	582.96371	S	2809.31326	1405.16027	937.10927	25
17	1861.90352	931.45540	621.30602	D	2722.28123	1361.64425	908.09859	24
18	1962.95120	981.97924	654.98858	T	2607.25428	1304.13078	869.75628	23
19	2076.03527	1038.52127	692.68327	L	2506.20660	1253.60694	836.07372	22
20	2163.06730	1082.03729	721.69395	S	2393.12253	1197.06490	798.37903	21
21	2291.16227	1146.08477	764.39227	K	2306.09050	1153.54889	769.36835	20
22	2388.21504	1194.61116	796.74320	P	2177.99553	1089.50140	726.67003	19
23	2475.24707	1238.12717	825.75387	S	2080.94276	1040.97502	694.31910	18
24	2572.29984	1286.65356	858.10480	P	1993.91073	997.45900	665.30843	17
25	2703.34034	1352.17381	901.78496	M	1896.85796	948.93262	632.95750	16
26	2800.39311	1400.70019	934.13589	P	1765.81746	883.41237	589.27734	15
27	2899.46153	1450.23440	967.15869	V	1668.76469	834.88598	556.92641	14
28	2986.49356	1493.75042	996.16937	S	1569.69627	785.35177	523.90361	13
29	3114.55214	1557.77971	1038.85556	Q	1482.66424	741.83576	494.89293	12
30	3243.59474	1622.30101	1081.86976	E	1354.60566	677.80647	452.20674	11
31	3346.60393	1673.80560	1116.20616	C	1225.56306	613.28517	409.19254	10
32	3493.67235	1747.33981	1165.22897	F	1122.55387	561.78057	374.85614	9
33	3622.71495	1811.86111	1208.24317	E	975.48545	488.24636	325.83333	8
34	3723.76263	1862.38495	1241.92573	T	846.44285	423.72506	282.81913	7
35	3836.84670	1918.92699	1279.62042	L	745.39517	373.20122	249.13657	6
36	3992.94782	1996.97755	1331.65412	R	632.31110	316.65919	211.44188	5
37	4049.96929	2025.48828	1350.66128	G	476.20998	238.60863	159.40818	4
38	4164.99624	2083.00176	1389.00360	D	419.18851	210.09789	140.40102	3
39	4294.03884	2147.52306	1432.01780	E	304.16156	152.58442	102.05870	2
40				R	175.11896	88.06312	59.04450	1

Fig. 1. (A) Interspecies comparison of known Vasostatin-1 derived peptides, residues (8–47) in human (h), rat(r), mouse (m), bovine (b), and porcine (p). (B) MS spectra of V1DP. (C) MS/MS sequencing data represented in panels which in each case show predicted singly- and doubly-charged *b*-ions and *y*-ions arising from MS/MS fragmentation. Observed ions are highlighted in red or blue typeface. (For interpretation of the references to color in this figure legend, the reader is referred to the web version of this article.)

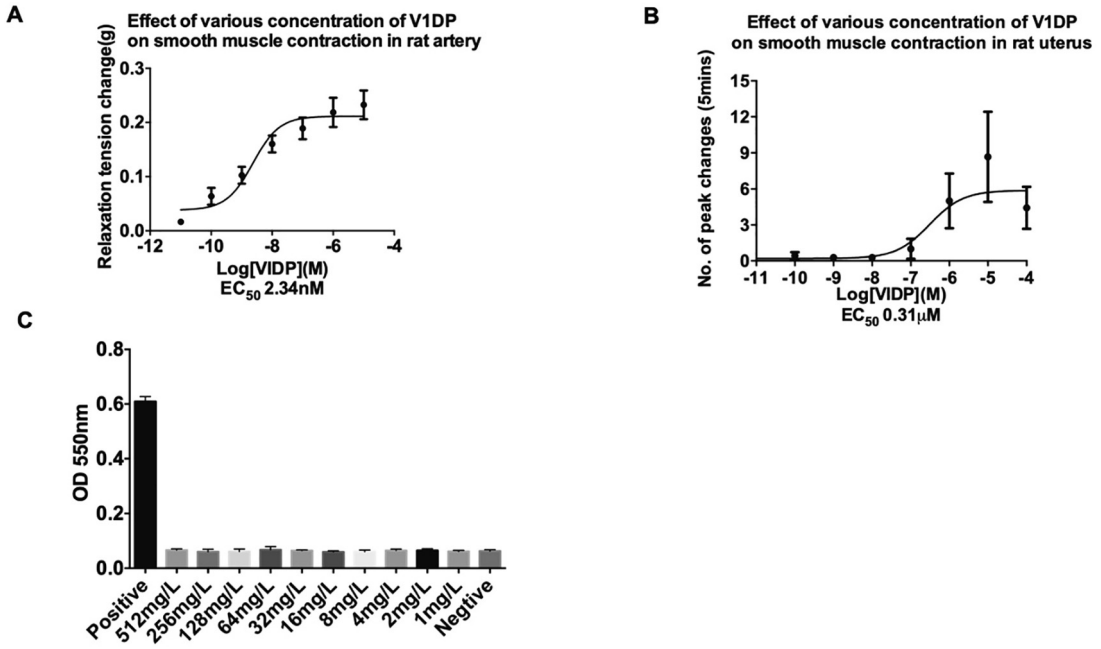

Fig. 2. Effect of various concentrations of V1DP on smooth muscle contraction frequency in A) rat artery and B) uterus. Each point represents the mean and standard error of six determinations (n = 3, six replicates). C) Haemolytic activities of V1DP following incubation with horse erythrocytes for 2 h.

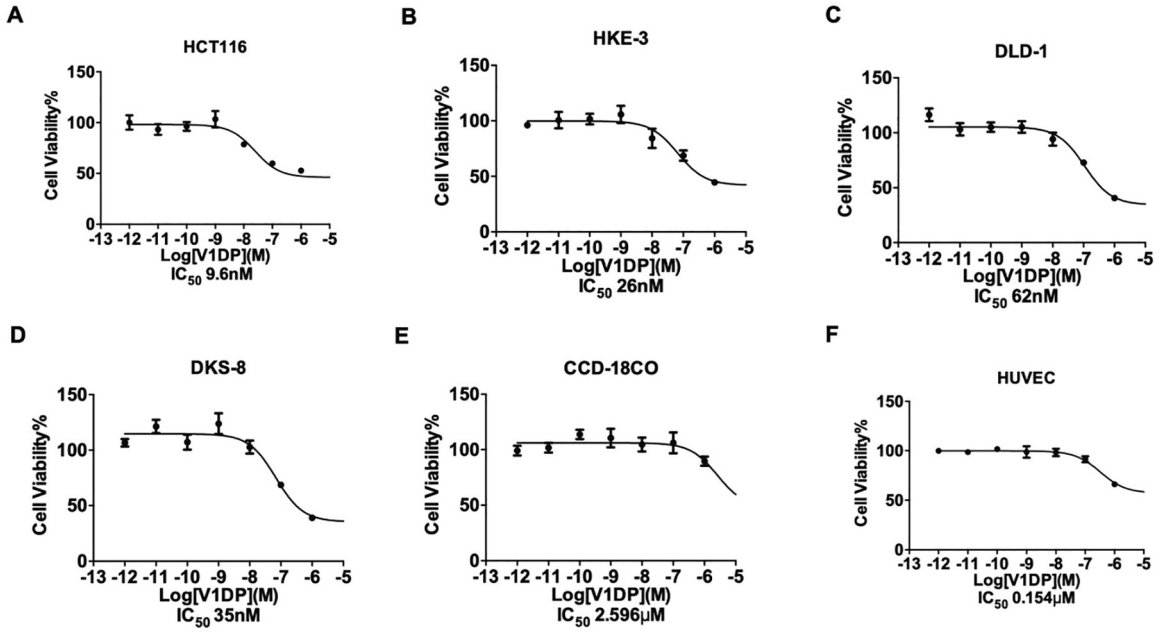

Fig. 3. MTT cell viability assay of V1DP on HCT116, HKE-3, DLD-1, DKS-8, CCD-18CO and HUVEC, respectively. The IC_{50} value of the anti-proliferative effects were presented accordingly.

3.4. Effect of V1DP on HUVEC migration and the anti-angiogenesis in vitro and vivo.

A wound healing assay was performed to determine the potential effect of V1DP on cell migration. After a 24-hour real-time observation, the HUVEC cell migration was effectively inhibited after treated with 10 μM V1DP and selective images were shown in Fig. 4A, while the 1 μM didn't show a significant inhibitory effect. Similar cases were also observed in the tube formation assay (Fig. 4B). Pretreatment of HUVEC with 10 μM V1DP for 6 h significantly inhibited HUVEC tube formation on matrigel while the inhibitory effect of 1 μM was much weaker. The inhibitory effect of 10 μM V1DP was similar to the positive control Cilengtide, a cyclic RGD pentapeptide that is recognized as a positive anti-angiogenic small molecular in cancer treatment [23]. The anti-angiogenesis effect of V1DP was further validated on the vascular development of zebrafish larvae (Fig. 5). V1DP was able to suppress the formation of intersegmental vessels (ISV) at the concentration of 50–100 μM and subintestinal vessels (SIV) in the zebrafish larvae at the concentration of 25–100 μM.

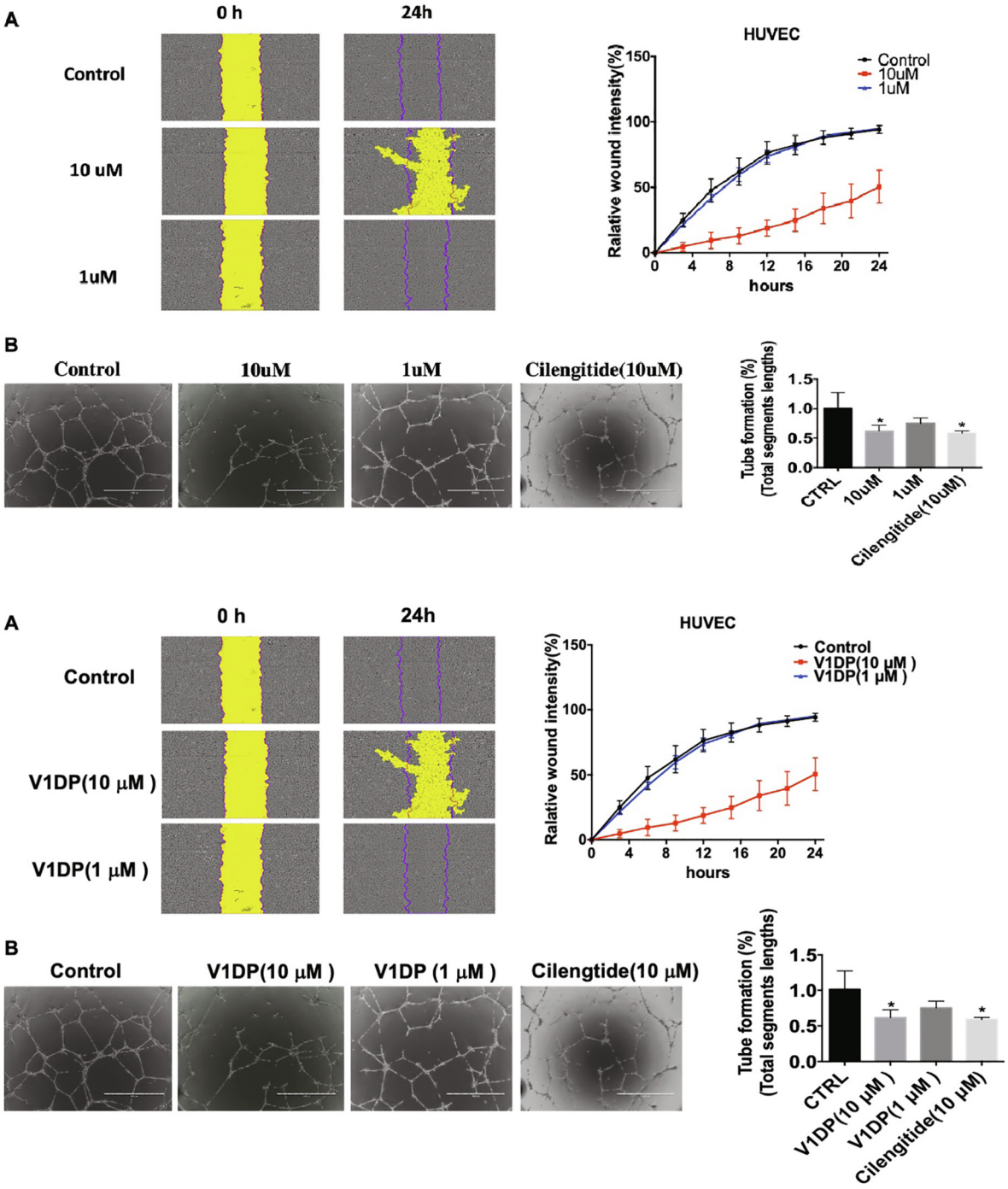

Fig. 4. A) Cell migration was measured in real-time by wound closure over 24 h using the IncuCyte, mean SD (error bars, n = 9). The migration rate was quantified by relative round intensity. B) HUVEC were pretreated with 10 μM V1DP, 1 μM V1DP, and 10 μM cilengitide as a positive comparison group. The tube formation was measured by the Angiogenesis Analyzer for ImageJ (*$p < 0.05$).

3.5. V1DP suppressed VEGF-induced ERK activation pathway

VEGFR2 is necessary for VEGF-stimulated endothelial proliferation and angiogenesis [24]. The activation of the VEGF downstream p42/44 MAP kinase pathway can induce cell proliferation and migration and induce the proangiogenic effect. In order to determine the potential effect of V1DP in anti-angiogenesis, the HUVEC cells were pretreated with V1DP at the 10 μM (the effective concentration in vitro test) for 6 h. The phosphorylation of ERK and VEGFR2 was inhibited after V1DP treatment, which suggests that the anti-angiogenesis effect of V1DP might involve the inhibition of VEGF-induced MAPK signaling (Fig. 6).

3.6. Peptide and protein modeling

The SWISS-MODEL structure of the V1DP has a helix-loop-helix fold as shown in Fig. 7. The RMSD analysis of the trajectory showed that the peptide structure was equilibrated in about 90 ns, reaching an average Cα RMSD of 0.41 ± 0.07 nm. Sidechain fluctuations were observed, mainly at the two ends of the peptide and the loop

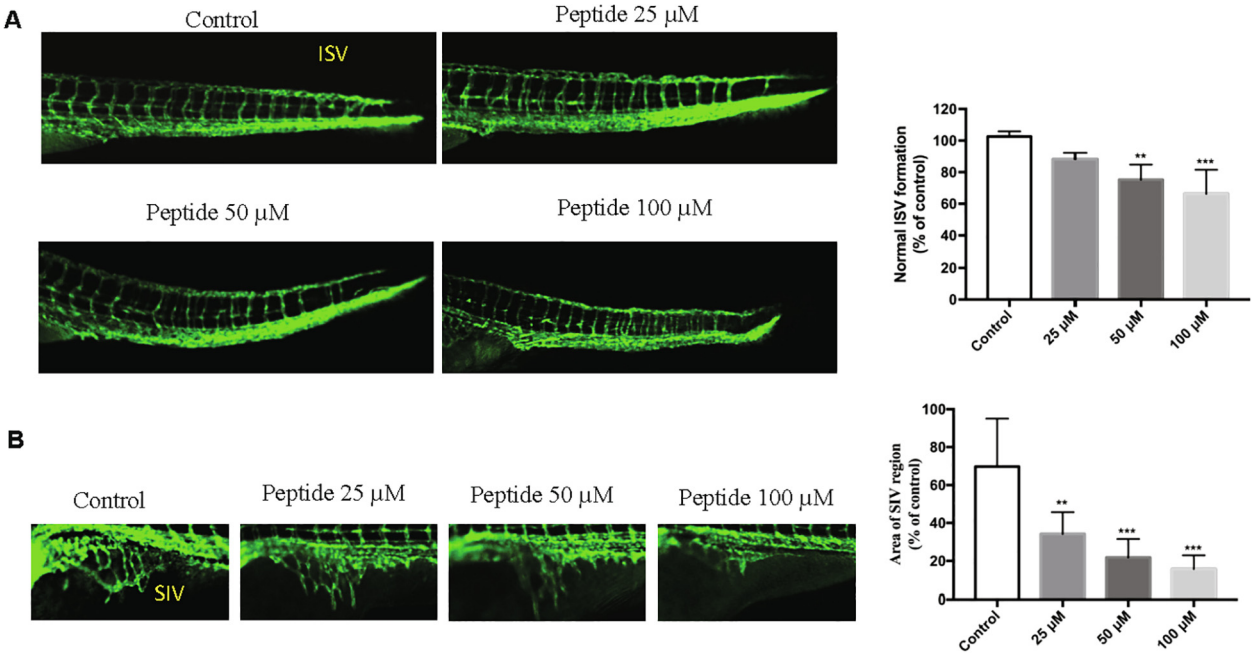

Fig. 5. Effects of VIDP on zebrafish angiogenesis. Fluorescent images of A) ISV and B) SIV in the zebrafish embryos incubated with PBS (Ctrl: vehicle-control), VIDP (25 μM, 50 μM, 100 μM) for 24 h. The quantification of ISV formation and SIV area were presented in the right panel respectively. All values are presented as means ± SD (n = 12). **P < 0, ***P < 0.005.

region between the residues 19 and 30. The peptide structure with high stability can be attributed to the strong Cys10-Cys31 disulfide bond that tightly told the two helices together. Interestingly, the equilibrated structure exhibits a non-polar surface on one side and a highly negatively charged surface (Glu6, Glu13, Asp17, Glu30, and Glu39) on the other side.

To prepare for docking, we performed MD simulations of the kinase domain models, one of which is in the JM-in state and the other in the JM-out state. Both models were well equilibrated in 200 ns. The Cα RMSD of the JM-in model has an average of 0.20 ± 0.04 nm, and the JM-out model has 0.24 ± 0.02 nm.

3.7. Identification of peptide binding sites in the kinase domain of VEGFR2

In order to identify potential binding sites in the protein and the initial binding mode of the peptide, we used an ensemble of protein conformations generated from MD to perform docking simulations. For the six representative protein conformations of the JM-in state, the 5 lowest energy predicted poses of the peptide were found to bind to the surface of the protein, except for one that is docked at the catalytic domain (CD). This one has a ZDOCK score of 13.66 kcal/mol, which is the second highest binding energy in the list (refer as S1-CA). For the JM-out state, of the 11 lowest energy predictions, in 6 of them the peptide was docked to the RDP domain. The binding mode of the peptide that has the highest ZDOCK score of 13.68 kcal/mol was identified (refer as S2-RDP). It is worth noting that the peptide was only docked to the CD and the surface of the protein, but not the RDP, when the protein is in the JM-in state. On the contrary, when the protein is in the JM-out state, the peptide was only docked to the RDP and the protein surface, but not the CD. This may hint that the V1DP peptide has a preferential binding location depending on the JM position of the protein. Two predicted complexes, S1-CA and S2-RDP were selected to continue with MD simulation to check for the stability of the binding. Previously, we had also simulated a representative surface-bound peptide, but it was diffused away in a short simulation time.

3.8. Protein-peptide binding analysis

As shown in Fig. 8, the MD results demonstrated that the peptide can stably bind to the CA and RDP of the protein because the peptide did not leave its binding region during the entire 100 ns simulation period. By visual inspection, it can be seen that the peptide is packed tightly at both the CD and RDP binding sites, with its non-polar surface facing to the pocket and the charged surface exposed to the solvent. Indeed, the bound peptide has much lower RMSD than its free form in solution. In S1-CD and S2-RDP, the average Cα RMSD of the peptide (including only residue 7 to 36, i.e. without the terminal coils) is 0.12 ± 0.02 nm and 0.14 ± 0.02 nm, respectively. In contrast, the unbound peptide has the average Cα RMSD of 0.30 ± 0.13 nm. The protein also showed excellent stability in both systems with the average Cα RMSD in S1-CD and S2-RDP being 0.22 ± 0.02 and 0.21 ± 0.04, respectively.

The binding free energies between the protein and peptide, and their energetic components are shown in Table 1. We can see that the van der Waals (E_{vdw}) and electrostatics (E_{elec}) energies between protein and peptide are negative, but the electrostatic contribution to the solvation free energy (E_{gb}) is a large positive value. This reveals that binding of the peptide to the protein involves large energetic penalty on the desolvation of the peptide, however, this loss is overcompensated by the sum of the van der Waals and electrostatics interactions between the protein and peptide. Taken the entropic term into account, the final free energy of binding ΔG, computed by MM/GBSA, is −12.63 kcal/mol for S1-CD and −21.61 kcal/mol for S2-RDP. Therefore, we can conclude that the peptide binds to the RDP of the protein with a higher affinity than to the CD and a difference them is about 9 kcal/mol.

We examined the hydrogen-bond and hydrophobic interaction types in the bound complex using the protein–ligand interaction profiler (PLIP) [25]. As shown in Fig. 9, the protein was found to form a few highly stable hydrogen bonds (contact frequency =>

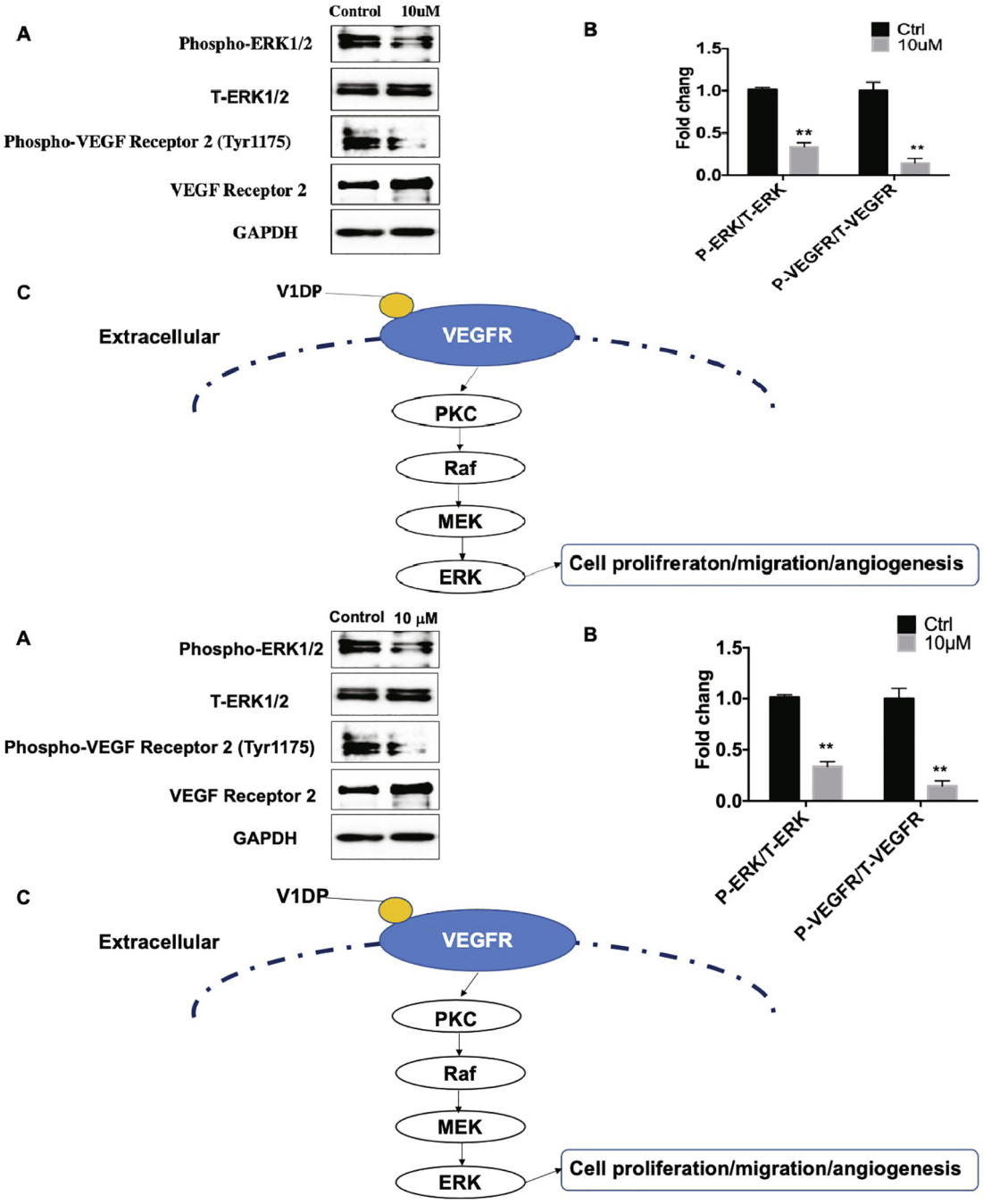

Fig. 6. A) Western blotting analysis for levels of phosphorylated ERK1/2, total ERK1/2, phosphorylated VEGFR2, total VEGFR2, in HUVEC where GAPDH was used as a reference. The cells were treated with/without 10 μM for 6 h before protein extraction. B) Quantification of the effect of V1DP on ERK and VEGFR phosphorylation. C) Schematic illustration of potential mechanisms of V1DP in angiogenesis.

1.0) with the peptide. For the S1-CA system, residues Arg929 and Thr926 of the protein were found always interacted with Gln29 and Met25 of the peptide, respectively. Deeper in the binding site, the protein residues Arg929 and Arg1051 interacted with the residues Val27 and Pro22 over 70% of the time. Interestingly, protein residues at the core of the catalytic site were found to form hydrophobic interactions with the peptide non-polar residues Leu19, Pro24, Leu35, and Val27 in 80% to 40% of the time. It should be pointed out that the DFG-motif residue, Phe1047, was found to form moderate hydrophobic interaction with the peptide residue Pro22 in 60% of the time (also see Fig. 8, upper panel, for the illustration of the aromatic rings interaction of Phe1047-Pro22). This binding analysis suggests that the V1DP peptide may potentially lock the protein in its inactivated state and inhibit the biological function of the protein via binding to its CD.

Similarly, for the S2-RDP system, a number of protein residues formed highly stable hydrogen bond with the peptide, including Arg1027 and Asp1028, which are at the bottom of the RDP pocket. Here, the DFG-motif residue, Asp1046, and the neighboring residue Glu885, together attracted the peptide residue Lys21 to the centre of the RDP. In an alternating fashion, these two residues maintained a close distance of about 0.17 nm to Lys21, thus exerting a very strong attractive force to the peptide (see Fig. 8, lower panel, for the illustration). Regarding the hydrophobic interactions, a

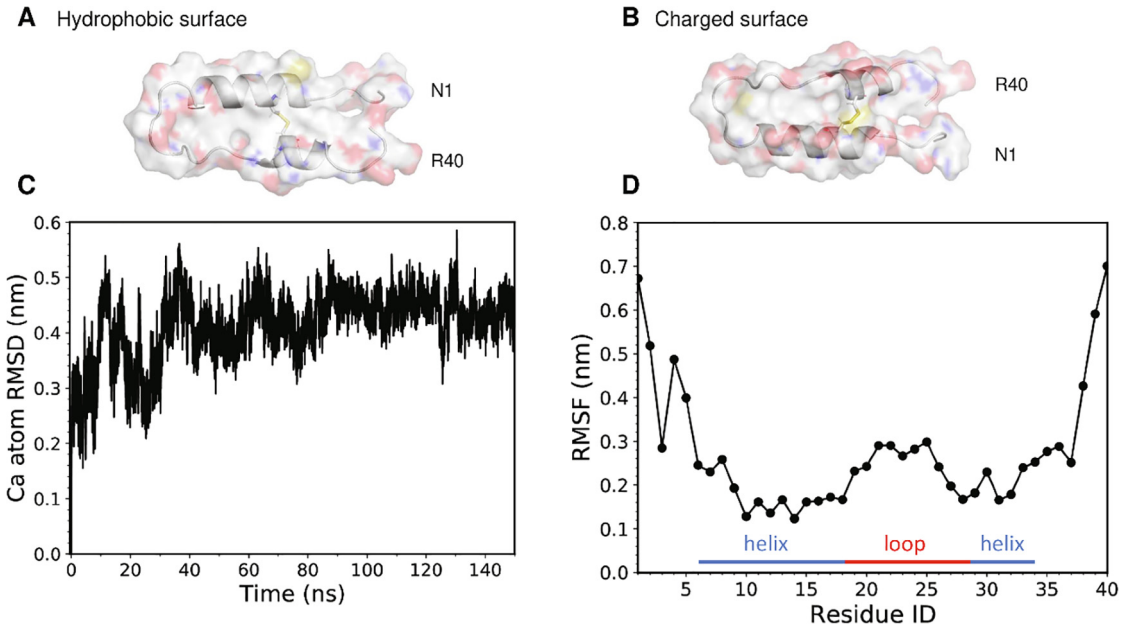

Fig. 7. The equilibrated V1DP at 150 ns: A) the non-polar surface and B) negatively charged surface. C) The root-mean-squared deviation (RMSD) and D) root-mean-squared fluctuation of the peptide simulated in the water box.

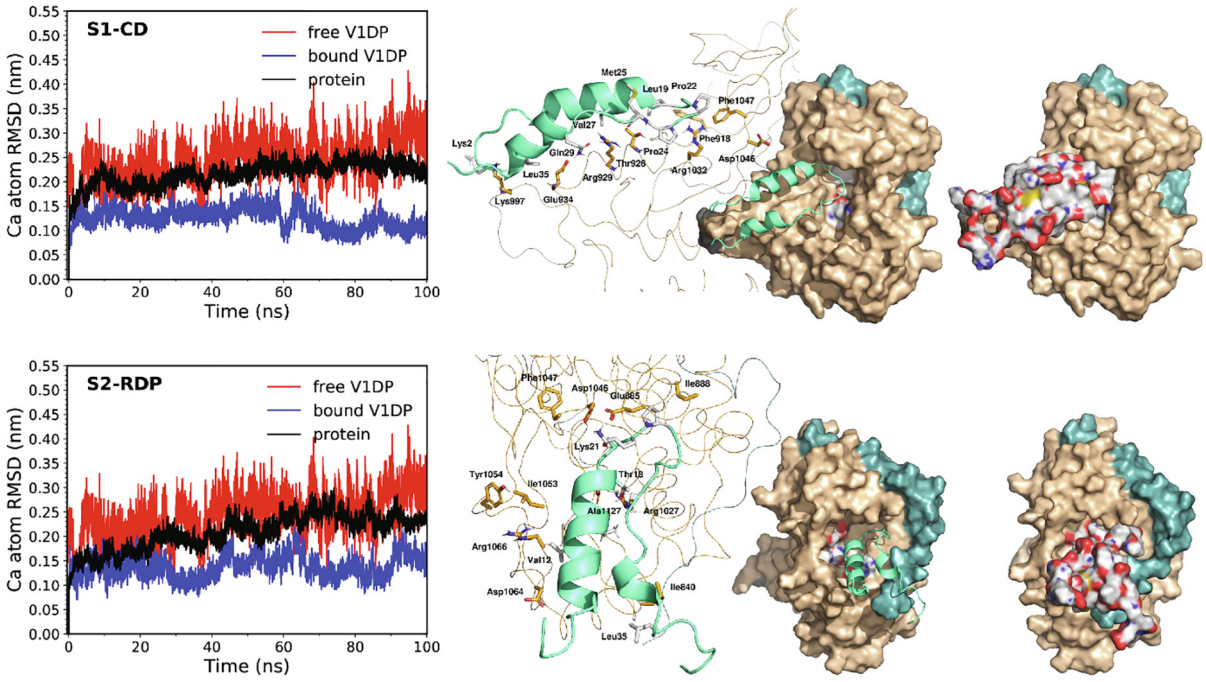

Fig. 8. Left panel: The Cα RMSDs of the peptide and protein in S1-CD and S2-RDP with respect to their initial structures. The free peptide RMSD simulated in solution was displayed as a reference. For both peptide and protein, only the non-loop/non-terminal regions were included in the calculations. Right panel: Snapshots of the complex at 100 ns; the peptide is shown in cartoon drawing with light-green color, or surface drawing with element-specific coloring (C and H: white, N: blue, O: red, S: yellow), the protein in wheat color with the long JM domain in teal color. (For interpretation of the references to color in this figure legend, the reader is referred to the web version of this article.)

number of pocket residues, Asp1064, Thr1054, Ile888, Ile1053, Arg1066, Ile804, etc. had similar interacting time (40–50%) with the peptide. Therefore, based on the docking and simulation results, it is likely that V1DP preferentially binds to the VEGFR2 kinase domain at the RDP pocket when the protein is in the JM-out state, while it binds to the CD pocket when the protein is in the JM-in state. The strong protein-peptide binding is mainly driven by electrostatics interactions and moderately by van der Waals interactions between the protein and peptide.

4. Discussion

CgA-related polypeptides are considered as serum biomarker for neuroendocrine tumour patients, most of the peptides have

Table 1
Binding free energies of the protein-peptide complex computed using MM/GBSA.

Energy component	S1-CD	S2-RDP
E_{vdw}	−98.95 ± 1.25	−84.60 ± 1.31
E_{elec}	−366.41 ± 6.61	−282.04 ± 5.35
E_{gb}	420.23 ± 6.59	313.63 ± 4.46
E_{surf}	−15.37 ± 0.19	−14.33 ± 0.16
ΔH	−60.50 ± 1.12	−67.34 ± 1.68
−TΔS	47.88 ± 7.98	45.73 ± 8.60
ΔG	−12.63	−21.61
Major interacting protein residues	W918, T926, R929, E934, K997, R1032, W1047, R1051	I804, I888, R1027, D1028, W1047, I1053, Y1054, D1064, R1066

Energy is in kcal/mol. Standard errors of mean were estimated directly by the gmx_MMPBSA program.
E_{vdw} & E_{elec}: van der Waals and electrostatics energy contributions from the molecular mechanics force field; E_{gb}: electrostatic contribution to the solvation free energy calculated by GB; E_{surf}: non-polar energy contribution to the solvation free energy; −TΔS: interaction entropy approximation; ΔG: the total binding free energy.

inhibitory roles in endocrine and vascular systems [26]. Neuroendocrine tumours can arise in most parts of the human body and these tumours may produce specific hormones that induce some specific tumour syndromes. The diagnostic approach for neuroendocrine tumours strongly depends on clinical hormone assays, nuclear medicine imaging and radiological imaging [26]. Those hormone and peptide secretions are synthesized as precursors that contain the biologically active peptides [27]. Many of these peptides may contribute to special clinical tumour syndromes or involved in regulating the tumor microenvironment, including fibroblasts and endothelial cells migration and adhesion.

CgA is the member of a family of acidic secretory proteins widely distributed in endocrine and neuroendocrine cells and sympathetic neurons and other neuroendocrine cells distributed along the gastrointestinal tract [28,29]. The significance of the CgA and its derived peptides as a prognostic marker in neuroendocrine tumours has been well recognized [30,31]. They are also active in cardiovascular, immunometabolic regulation such as hypertension, rheumatoid arthritis, heart failure, renal failure and inflammatory bowel disease [6]. Our research teams have been focused on the track research of CgA derived peptides in the last decades. We observed that CgA and its derived peptides are actively processed in pancreatic beta cells of insulinoma, also found in mid-gut carcinoid and phaeochromocytoma where tumors express appropriate prohormone convertases [31].

Among these derived peptides, Vasostatin-1 was named based on its inhibitory effects on blood vessel contractility in 1992 [32]. Later, more inhibitory activities were observed with tumor angiogenesis and a tumour vessel architecture modulator [7]. Vasostatin-1 works as cardio regulatory hormones that can depress myocardial contractility and relaxation, counteract the β-adrenergic induced positive inotropism, and modulate coronary tone mainly via a nitric oxide-dependent mechanism[33]. Meanwhile, it can inhibit the TNF induced endothelial cell activation and permeability, including the phosphorylation of p38 MAP kinase [33].

In this study, V1DP was derived from N-terminal fragment of Vasostatin I (residues 8–47), Overviewing the typical primary structure of V1DP, the three typical functional structures, RGD and KGD, and a disulphide bridge formed by two cysteine residues at amino acid positions 17 and 38 might play the main role in determining the functions of the peptide. These three functional domains are also the typical functional structure of Vasostatin-1, which have high degrees of interspecies conservation (Fig. 1A). The interaction of RGD sequences in adhesive glycoproteins were found to be platelet receptor recognition sites on these adhesive ligands and are thought to be crucial to normal platelet function [34,35]. There are coincidentally many cysteine-rich, RGD-containing snake venom peptide disintegrins [35]. The two cysteine residues (Cys17-Cys38) in Vasostatin-1 interact to form an intra-molecular disulphide loop which is required for sorting to secretory granules and homodimerization [36]. The sequence of the disulphide loop, located between the KGD and RGD regions, is a unique hydrophobic region within the entire peptide and has been shown to play an important role in determining its secondary

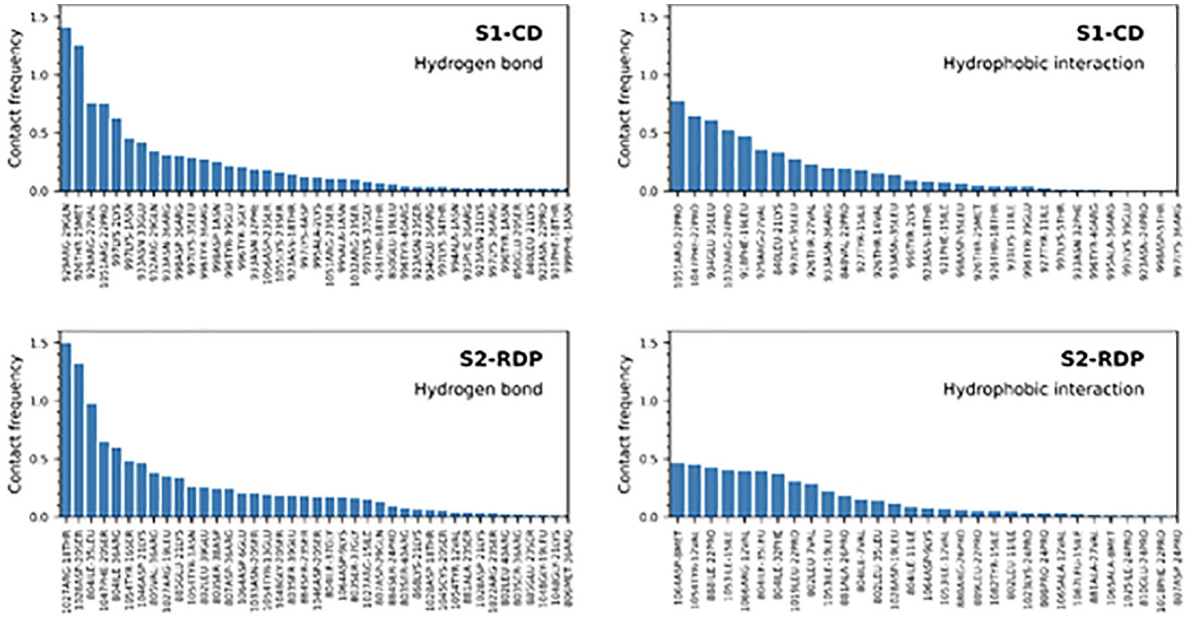

Fig. 9. Hydrogen-bonding and hydrophobic interactions observed in the last 40 ns simulation of the bound V1DP kinase domain complex in the S1-CD and S2-RDP systems. In each case, totally 400 frames were analyzed. The contact frequency was computed as the total number of specific interaction occurred divided by the total number of frames. As two residues may form more than one hydrogen bonds between different atom pairs, the contact frequency can be >1.

structural properties and also as a necessity for its biological functions [36]. It also displays a 32% identity and 64% similarity with a region of the fibronectin type III-9 domain of tenascin, an extracellular matrix protein that is conserved in all vertebrates [37].

We found that this novel peptide exerted a dose-dependent relaxation of rat arterial smooth muscle and also induce the contraction activity of rat uterus smooth muscle. It inhibited cancer cell proliferation and HUVEC cell migration and exhibited an anti-angiogenesis effect both *in vitro* and *in vivo.* The western blot results in Fig. 6 indicated that the phosphorylation of ERK and VEGFR2 was inhibited after V1DP treatment, which suggests that the V1DP might block the VEGFR signaling pathway. Angiogenesis is involved in tumor growth, macular degeneration, retinopathy and other diseases. VEGF stimulates angiogenesis by binding to specific receptors (VEGFRs) on the surface of vascular endothelial cells. VEGFRs are receptor tyrosine kinases that, like the platelet-derived growth factor receptors (PDGFRs), contain a large insert within the kinase domain [38]. There are many studies on the role of VEGF in new blood vessel formation in these extremely well-vascularized tumors and of its role in metastasis of the tumour. Our docking and simulation results indicated that V1DP might bind to the active site and RDP of the VEGFR2 kinase domain and subsequently inhibited the activation of the VEGF signaling pathway. V1DP exhibited a highly complementary shape to both pockets. However, the free energy of binding of the peptide in the RDP is −21.61 kcal/mol, which is about 9 kcal/mol lower than that of the CA, indicating that the peptide has a stronger binding force in RDP. V1DP showed a similar dose inhibitory effect as cilengitide, a cyclic RGD pentapeptide that is recognized as a positive anti-angiogenic small molecular in cancer treatment. These results further support the structural characterization of V1DP in the anti-anagenesis effect. In addition, V1DP showed selective cytotoxicity only against cancer cell without any haemolytic toxicity.

Taken together, all the in vitro, in vivo and *in silico* data obtained in this study indicate that V1DP is a water-soluble and biologically stable peptide and has the potential to develop as an anti-angiogenic drug for cancer treatment after further structural–functional optimization.

Funding

This study was supported by the Science and Technology Development Fund, Macau SAR (File no. 019/2017/A1 and 0055/2019/A1). All simulations were performed at the High-Performance Computing Cluster (HPCC) provided by the Information and Communication Technology Office (ICTO) of the University of Macau (UM). Thanks to the Biological Imaging & Stem Cell Core (BISCC) in the Faculty of Health Sciences (FHS) UM to provide the imaging facility and services.

Authors contributions

RW, QW, NA, SS and LW carried out the experiments and performed the MD statistical analysis. RW and SS drafted the manuscript. WG supervised the in vivo work. TC, MZ, CS and HFK participated in the design of the study. HFK and RDY revised the manuscript. All authors read and approved the final manuscript.

Declaration of Competing Interest

The authors declare that they have no known competing financial interests or personal relationships that could have appeared to influence the work reported in this paper.

References

[1] Blaschko H, Comline RS, Schneider FH, Silver Marian, Smith AD. Secretion of a chromaffin granule protein, chromogranin, from the adrenal gland after splanchnic stimulation. Nature 1967;215(5096):58–9.
[2] Eissa N, Hussein H, Kermarrec L, Ali AY, Marshall A, Metz-Boutigue M-H, et al. Chromogranin-A regulates macrophage function and the apoptotic pathway in murine DSS colitis. J Mol Med 2018;96(2):183–98.
[3] D'amico MA, Ghinassi B, Izzicupo P, Manzoli L, Di Baldassarre A. Biological function and clinical relevance of chromogranin A and derived peptides. Endocrine Connect 2014;3:R45–R54.
[4] Crippa L, Bianco M, Colombo B, Gasparri AM, Ferrero E, et al. A new chromogranin A–dependent angiogenic switch activated by thrombin. Blood J. Am. Soc. Hematol. 2013;121:392–402.
[5] Ratti S, Curnis F, Longhi R, Colombo B, Gasparri A, Magni F, et al. Structure-activity relationships of chromogranin A in cell adhesion: identification of an adhesion site for fibroblasts and smooth muscle cells. J Biol Chem 2000;275(38):29257–63.
[6] Mahata SK, Corti A. Chromogranin A and its fragments in cardiovascular, immunometabolic, and cancer regulation. Ann N Y Acad Sci 2019;1455(1):34–58.
[7] Braga F, Ferraro S, Mozzi R, Dolci A, Panteghini M. Biological variation of neuroendocrine tumor markers chromogranin A and neuron-specific enolase. Clin Biochem 2013;46(1-2):148–51.
[8] Angelone T, Quintieri AM, Brar BK, Limchaiyawat PT, Tota B, et al. The antihypertensive chromogranin a peptide catestatin acts as a novel endocrine/paracrine modulator of cardiac inotropism and lusitropism. Endocrinology 2008;149:4780–93.
[9] Cerra MC, Iuri L, Angelone T, Corti A, Tota B. Recombinant N–terminal fragments of chromogranin–a modulate cardiac function of the Langendorff–perfused rat heart. Basic Res Cardiol 2006;101(1):43–52.
[10] Gasparri A, Sidoli A, Sanchez LP, Longhi R, Siccardi AG, Marchisio PC, et al. Chromogranin A fragments modulate cell adhesion Identification and characterization of a pro-adhesive domain. J Biol Chem 1997;272(33):20835–43.
[11] Wang J, Han X, Yang H, Lu Li, Wu Yu, Liu X, et al. A novel RGD-toxin protein, Lj-RGD3, from the buccal gland secretion of Lampetra japonica impacts diverse biological activities. Biochimie 2010;92(10):1387–96.
[12] Maheshwari G, Brown G, Lauffenburger DA, Wells A, Griffith LG. Cell adhesion and motility depend on nanoscale RGD clustering. J Cell Sci 2000;113:1677–86.
[13] Shi D, Luo Yu, Du Q, Wang L, Zhou M, Ma J, et al. A novel bradykinin-related dodecapeptide (RVALPPGFTPLR) from the skin secretion of the fujian large-headed frog (Limnonectes fujianensis) exhibiting unusual structural and functional features. Toxins 2014;6(10):2886–98.
[14] Lyu P, Ge L, Ma R, Wei R, McCrudden CM, Chen T, et al. Identification and pharmaceutical evaluation of novel frog skin-derived serine proteinase inhibitor peptide–PE-BBI (Pelophylax esculentus Bowman-Birk inhibitor) for the potential treatment of cancer. Sci Rep 2018;8(1). https://doi.org/10.1038/s41598-018-32947-5.
[15] Guo X, Ma C, Du Q, Wei R, Wang L, Zhou M, et al. Two peptides, TsAP-1 and TsAP-2, from the venom of the Brazilian yellow scorpion, Tityus serrulatus: evaluation of their antimicrobial and anticancer activities. Biochimie 2013;95(9):1784–94.
[16] Wei R, Wong JPC, Lyu P, Xi X, Tong O, Zhang S-D, et al. In vitro and clinical data analysis of Osteopontin as a prognostic indicator in colorectal cancer. J Cell Mol Med 2018;22(9):4097–105.
[17] Ai N, Chong C-M, Chen W, Hu Z, Su H, Chen G, et al. Ponatinib exerts anti-angiogenic effects in the zebrafish and human umbilical vein endothelial cells via blocking VEGFR signaling pathway. Oncotarget 2018;9(62):31958–70.
[18] Lamiable A, Thévenet P, Rey J, Vavrusa M, Derreumaux P, et al. PEP-FOLD3: faster de novo structure prediction for linear peptides in solution and in complex. Nucleic Acids Res 2016;44:W449–54.
[19] Waterhouse A, Bertoni M, Bienert S, Studer G, Tauriello G, et al. SWISS-MODEL: homology modelling of protein structures and complexes. Nucleic Acids Res 2018;46:W296–W303.
[20] Capelli AM, Costantino G. Unbinding pathways of VEGFR2 inhibitors revealed by steered molecular dynamics. J Chem Inf Model 2014;54(11):3124–36.
[21] Wu G, Robertson DH, Brooks CL, Vieth M. Detailed analysis of grid-based molecular docking: a case study of CDOCKER—a CHARMm-based MD docking algorithm. J Comput Chem 2003;24(13):1549–62.
[22] Jo S, Kim T, Iyer VG, Im W. CHARMM-GUI: a web-based graphical user interface for CHARMM. J Comput Chem 2008;29(11):1859–65.
[23] Mas-Moruno C, Rechenmacher F, Kessler H. Cilengitide: the first anti-angiogenic small molecule drug candidate. Design, synthesis and clinical evaluation. Anti-Cancer Agents Med Chem (Formerly Curr Med Chem-Anti-Cancer Agents) 2010;10(10):753–68.
[24] Karkkainen MJ, Petrova TV. Vascular endothelial growth factor receptors in the regulation of angiogenesis and lymphangiogenesis. Oncogene 2000;19(49):5598–605.
[25] Salentin S, Schreiber S, Haupt VJ, Adasme MF, Schroeder M. PLIP: fully automated protein–ligand interaction profiler. Nucleic Acids Res 2015;43(W1):W443–7.
[26] de Herder WW. Biochemistry of neuroendocrine tumours. Best Pract Res Clin Endocrinol Metab 2007;21(1):33–41.

[27] Wilson HE, White A. Prohormones: their clinical relevance. Trends Endocrinol Metab 1998;9(10):396–402.
[28] Pérez JÁD, Freixes MC. Chromogranin A and neuroendocrine tumors. Endocrinología y Nutrición (English Edition) 2013;60:386–95.
[29] Winkler H, Fischer-Colbrie R. The chromogranins A and B: the first 25 years and future perspectives. Neuroscience 1992;49(3):497–528.
[30] Xie J, Chen P, Xie H, Sun Y, Huang Z, Wei R, et al. Exploration of gastric neuroendocrine carcinoma (GNEC) specific signaling pathways involved in chemoresistance via transcriptome and in vitro analysis. Comput Struct Biotechnol J 2020;18:2610–20.
[31] Orr DF, Chen T, Johnsen AH, Chalk R, Buchanan KD, Sloan JM, et al. The spectrum of endogenous human chromogranin A-derived peptides identified using a modified proteomic strategy. Proteomics 2002;2(11):1586–600.
[32] Aardal S, Helle KB. The vasoinhibitory activity of bovine chromogranin A fragment (vasostatin) and its independence of extracellular calcium in isolated segments of human blood vessels. Regul Pept 1992;41(1):9–18.
[33] Blois A, Srebro B, Mandalà M, Corti A, Helle KB, Serck-Hanssen G. The chromogranin A peptide vasostatin-I inhibits gap formation and signal transduction mediated by inflammatory agents in cultured bovine pulmonary and coronary arterial endothelial cells. Regul Pept 2006;135(1-2):78–84.
[34] Yeh C-H, Peng H-C, Yih J-B, Huang T-F. A new short chain RGD-containing disintegrin, accutin, inhibits the common pathway of human platelet aggregation. Biochimica et Biophysica Acta (BBA)-General Subjects 1998;1425(3):493–504.
[35] Gould RJ, Polokoff MA, Friedman PA, Huang T-F, Holt JC, Cook JJ, et al. Disintegrins: a family of integrin inhibitory proteins from viper venoms. Proc Soc Exp Biol Med 1990;195(2):168–71.
[36] Benedum UM, Baeuerle PA, Konecki DS, Frank R, Powell J, Mallet J, et al. The primary structure of bovine chromogranin A: a representative of a class of acidic secretory proteins common to a variety of peptidergic cells. EMBO J 1986;5(7):1495–502.
[37] Spring J, Beck K, Chiquet-Ehrismann R. Two contrary functions of tenascin: dissection of the active sites by recombinant tenascin fragments. Cell 1989;59(2):325–34.
[38] McTigue MA, Wickersham JA, Pinko C, Showalter RE, Parast CV, Tempczyk-Russell A, et al. Crystal structure of the kinase domain of human vascular endothelial growth factor receptor 2: a key enzyme in angiogenesis. Structure 1999;7(3):319–30.